RSC Advances

PAPER

Cite this: *RSC Adv.*, 2018, **8**, 32558

Alginic acid aquagel as a template and carbon source in the synthesis of $Li_4Ti_5O_{12}$/C nanocomposites for application as anodes in Li-ion batteries†

Sanghoon Kim, [a] Johan G. Alauzun, [a] Nicolas Louvain, [ab] Nicolas Brun,[a] Lorenzo Stievano, [ab] Bruno Boury,[a] Laure Monconduit [ab] and P. Hubert Mutin *[a]

We report here a simple process for the synthesis of $Li_4Ti_5O_{12}$(LTO)/carbon nanocomposites by a one-pot method using an alginic acid aquagel as a template and carbon source, and lithium acetate and TiO_2 nanoparticles as precursors to the LTO phase. The carbon content can be tuned by adjusting the relative amount of alginic acid. The obtained materials consist of nanosized primary particles of LTO (30 nm) forming micron-sized aggregates covered by well-dispersed carbon (from 3 to 19 wt%). The homogeneous dispersion of carbon over the particles improves the electrochemical performance of LTO electrodes such as rate capability (>95 mA h g^{-1} at 40C) and cycling performance (>98% of retention after 500 cycles at 5C), even with only 3% of carbon black additive in the electrode formulation. With a simple and easily up-scalable synthesis, the LTO/carbon nanocomposites of this study are promising candidates as anode materials for practical application in lithium-ion batteries.

Received 11th July 2018
Accepted 30th August 2018

DOI: 10.1039/c8ra05928d

rsc.li/rsc-advances

Introduction

$Li_4Ti_5O_{12}$ (LTO) has been intensively investigated as a safe alternative to graphite for the negative electrode in high-power lithium-ion batteries (LIBs). The main advantages of LTO are its low cost, zero volume change during Li^+ intercalation and de-intercalation processes, remarkable cycling stability and excellent safety.[1–6] However, the main drawback for practical application in high-power lithium-ion batteries is its poor electronic conductivity (10^{-11} S m^{-1}), which results in poor performance at high rate. Several methods have been proposed to improve the electronic conductivity including heteroatom doping (*e.g.* Zr^{4+}, F^-)[7–11] or conductive carbon coating.[12–15] In addition, nanostructuring of the electrode material could provide a larger contact area between electrode and electrolyte, resulting in an improvement of Li^+ intercalation kinetics. Accordingly, LTO/C nanocomposites have recently attracted much attention because a performance improvement at high rate can be obtained due not only to enhanced electronic conductivity by the carbon but also to the faster Li^+ ion diffusion.[16–19] However, most works on the synthesis of such nanostructured LTO/C materials involve multiple-step sophisticated syntheses, which cannot be easily scaled up for industrial application.[14,20]

Solid-state synthesis is one of most common methods for the synthesis of electrode materials and it is well adapted to up-scaling. This method consists of mixing solid precursors by grinding or ball-milling, followed by a thermal treatment such as calcination or pyrolysis at high temperature.[21–23] However, a fine tailoring of LTO properties cannot be easily achieved by solid-state synthesis and the final materials generally suffer from uncontrollable particle growth, irregular agglomeration or even inhomogeneity from the presence of various impurity phases.[24–26] As a result, the electrochemical performance of such electrode materials is generally lower than that of nanostructured materials prepared through sol–gel or templating methods, especially at high charge–discharge rates.[3]

In the present work we propose to use an alginic acid aquagel as a carbon source and a complexing agent for the synthesis of LTO/C nanocomposites by a one-pot solid-state reaction involving lithium acetate and TiO_2 nanoparticles as precursors to the LTO phase. Homogenous dispersion of LTO precursors over the chelating alginic acid aquagel allowed the formation of a highly pure LTO phase and the uniform deposition of carbon over the LTO nanoparticles. The electrochemical performance of the LTO/carbon nanocomposites prepared by this easily upscalable method was greatly improved compared to commercial LTO, even with

[a]*Institut Charles Gerhardt Montpellier, UMR 5253 Univ. Montpellier-CNRS-ENSCM, Montpellier, France. E-mail: hubert.mutin@umontpellier.fr*

[b]*Réseau sur le Stockage Electrochimique de l'Energie (RS2E), CNRS, FR3459, 33 Rue Saint Leu, 80039 Amiens Cedex, France*

† Electronic supplementary information (ESI) available: Additional characterization of $Li_4Ti_5O_{12}$ materials and their electrochemical performance. See DOI: 10.1039/c8ra05928d

low amounts of carbon black as a conductive additive in electrode formulation.

Experimental

Materials

Titanium oxide nanoparticles (TiO_2, anatase, >99%) were purchased from Tronox. Lithium acetate dihydrate (LiOAc >98%) and alginic acid from brown algae were purchased from Sigma-Aldrich. Carbon black (Super P >99%) was purchased from Alfa Aesar. For comparison purposes, a commercially available sub-micronic LTO powder (denoted T-LTO) was obtained from Targray (Canada). Carbon black powders were dried in an oven at 65 °C before use. All other reagents were used without further purification.

Synthesis of LTO/C nanocomposites

LTO/C nanocomposites with various carbon content were synthesized by a one-pot solid state reaction. Depending on the weight of alginic acid reacted, LTO/C samples with different carbon contents were obtained (Table 1). For example, a LTO/carbon nanocomposite with 3 wt% of carbon was prepared as follows: 200 mg of alginic acid was gelled in water (10 mL) by heating at 90 °C for 2.5 h, followed by retrogradation at 4 °C for 24 h. Then, 479 mg of TiO_2 and 505 mg of LiOAc were added to the resulting aquagel and stirred for 2 h at room temperature. The water was removed by freeze drying, and the final LTO/carbon composite was obtained by pyrolysis at 800 °C (heating rate 1 °C min^{-1}) for 3 h under argon flow (50 mL min^{-1}). The samples are labeled LTO/C-*x*, where *x* stands for the carbon content (wt%). Besides, a carbon free LTO was also obtained by calcination of LTO/carbon composite at 500 °C for 5 h in air; this sample is labeled LTO/C-0.

Electrode preparation and half coin cell assembly

Electrodes with 3 different carbon black contents were prepared using LTO/C (active material), Super P (conductive carbon black) and PVDF (binder) in a mass ratio of 94 : 0 : 6, 91 : 3 : 6 or 88 : 6 : 6. These electrodes are thereafter referred to as LTO/C-*x*-CB-*y*, where *x* stands for the carbon content in the LTO/C nanocomposite and *y* for the amount of Super P added in the electrode formulation (*e.g.* LTO/C-3-CB-6). After stirring in *N*-methyl-2-pyrrolidone (NMP), the slurry was mixed using an agate grinding jar (1 h at 500 rpm), then tape casted uniformly at 150 μm onto a copper current collector (0.018 mm, >99.96%, Promoter) using a 3540 bird film applicator from Elcometer. Electrodes (diameter 12.7 mm) were cut with a disk cutter and then dried under vacuum at 90 °C for 15 h. The loading weight per electrode disk was ≈2.0 mg per disk. CR2032 coin-type cells were assembled in a glove box under Ar atmosphere (O_2 <0.5 ppm, H_2O <0.5 ppm), using lithium metal as both reference and counter electrode. The electrolyte was LP30 (1 M) $LiPF_6$ dissolved in a mixture of ethylene carbonate (EC) and dimethyl carbonate (DMC) (ratio EC : DMC = 1 : 1). Whatman glass fibre disks were used as separators. Besides, an electrode was also prepared using the commercial T-LTO sample, Super P, and PVDF in a mass ratio of 88 : 6 : 6 and denoted T-LTO-CB-6.

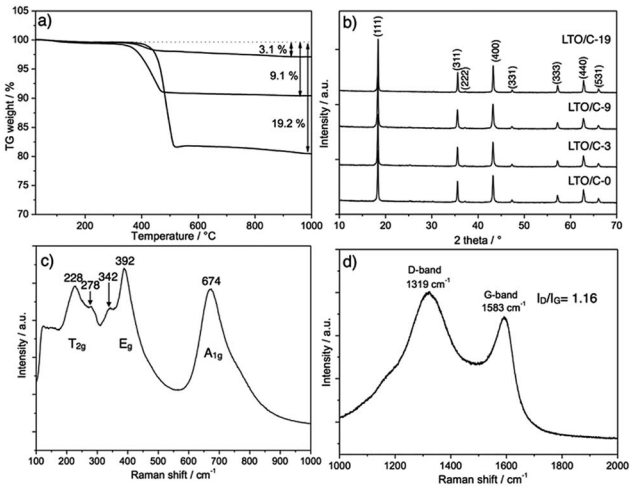

Fig. 1 (a) Determination of carbon content by TGA in air (heating rate 10 °C min^{-1}); (b) XRD patterns of LTO/C nanocomposites, (c) and (d) Raman spectra of LTO/C-3.

Characterization

XRD patterns were recorded using a PANalytical X'Pert Pro MPD diffractometer, with the Kα radiation of Cu ($\lambda = 1.5418$ Å) and a step size of 0.033° into the 10–80° interval. N_2 physisorption experiments were carried out at −196 °C on a Micromeritics 3Flex. The specific surface area was calculated by the BET (Brunauer–Emmett–Teller) method and the pore volume was calculated by the Barrett–Joyner–Halenda (BJH) method. Thermogravimetric analysis (TGA) was performed on a TG instrument (NETZSCH STA 409 PC) with a heating rate of 5 °C min^{-1} from 25 to 1000 °C. Scanning electron microscopy (SEM) images

Table 1 Influence of the alginic acid weight on carbon content in LTO/C

Sample	Alginic acid weight[a] (mg)	Carbon content[b] (wt%)
LTO/C-3	200	3.1
LTO/C-9	600	9.1
LTO/C-19	1300	19.2

[a] For 480 mg of TiO_2 and 500 mg of LiOA. [b] Determined by TGA in air of the LTO/C materials.

Table 2 Textural properties of LTO/C nanocomposites[a]

Sample	S_{BET} (m^2 g^{-1})	PV_{meso} (cm^3 g^{-1})	PV_{total} (cm^3 g^{-1})
LTO/C-19	87	0.04	0.08
LTO/C-9	46	0.05	0.05
LTO/C-3	21	0.05	0.06
LTO/C-0	<5	—	—

[a] S_{BET}: Specific surface area determined by BET method; PV_{total}: total pore volume at $P/P_0 = 0.99$; PV_{meso}: volume of mesopores between 2 and 50 nm determined by the BJH method.

were acquired with a Hitachi S-4800 electron microscope. Transmission electron microscopy (TEM) images were acquired using JEOL FX2200 microscope. Galvanostatic electrochemical characterizations were performed at room temperature on a BTS3000 instrument from Neware Battery in the 2.5–1.25 V voltage range *versus* Li^+/Li at different current densities. All the capacity data reported here are the average of at least 3 different experiments.

Results and discussion

Synthesis and characterization of LTO/C nanocomposites

A series of LTO/C nanocomposites with different carbon contents was obtained by mixing an alginic acid aquagel with TiO_2 nanoparticles and lithium acetate, followed by freeze-drying then pyrolysis at 800 °C. In this simple method, the carbon content in the final nanocomposites directly depends on the relative amount of alginic acid aquagel used in the synthesis, as shown in Table 1. The carbon content of LTO/C nanocomposites was determined by thermogravimetric analysis (TGA) (Fig. 1a). The carbon content for all materials is lower than the value calculated based on the typical carbonization yield of alginic acid (20%).[27] For example, the carbon content in C-LTO-3 was 3 wt% instead of 5 wt% for the calculated content. This could be due to the presence of TiO_2 or Li^+, which would catalyze unexpected decomposition or degradation of alginic acid during the carbonization (pyrolysis) step. Fig. 1b shows the XRD pattern of LTO/C nanocomposites with different carbon contents. In all cases, the XRD pattern indicated the formation of a pure LTO phase. The diffraction peaks at $2\theta = 18.4$, 35.6, 37.2 43.2, 47.3, 57.2, 62.8 and 66.1°, corresponding to the (111), (311), (222), (400), (331), (333), (440) and (531) planes, can be indexed to the cubic spinel phase of LTO (JCPDS no. 49-0207). No other peaks characteristic of impurities such as TiO_2 or Li_2TiO_3 were observed. On the other hand, small amounts of these impurities were detected in LTO synthesized without alginic acid (Fig. S1†). This suggests that the complexation of LTO precursors (LiOAc and TiO_2) by the carboxylic acid groups of the alginic acid aquagel favors the formation of a phase pure LTO. In addition, no characteristic peaks for carbon (around $2\theta = 27°$) were observed even for LTO/C-19 (*ca.* 19 wt% of carbon), indicating that the carbon of these nanocomposites was mostly amorphous. The size of the LTO crystallites estimated by the Scherrer equation was ≈36 nm, similar for all the LTO/C samples, even for LTO/C-0, which was obtained by calcination in air of LTO/C-3 at 500 °C.

The Raman spectra of the LTO/C nanocomposite with 3% of carbon (LTO/C-3) in the 100 to 1000 cm^{-1} range is shown in Fig. 1c. The peaks at 228, 278, 342, 392 and 674 cm^{-1} can be assigned to the five expected T_{2g}, E_g and A_{1g} modes for the spinel $O^7{}_h$ symmetry group.[28] No characteristic peaks for TiO_2 anatase (intense peak at 152 cm^{-1}) or rutile (intense peak at 413 cm^{-1})[29] were observed, confirming the high purity of the inorganic LTO phase in the nanocomposites. In the higher range (1000–2000 cm^{-1}) (Fig. 1d), the two strong and very broad bands around 1319 and 1583 cm^{-1} can be attributed to the in-plane vibrations of disordered amorphous carbon (D-band) and crystalline graphic carbon (G-band), respectively. From the width of these bands and the ratio of intensity of D-band to G-band (I_D/I_G), it can be suggested that the carbon in LTO/C-3 had a low degree of graphitization.[30]

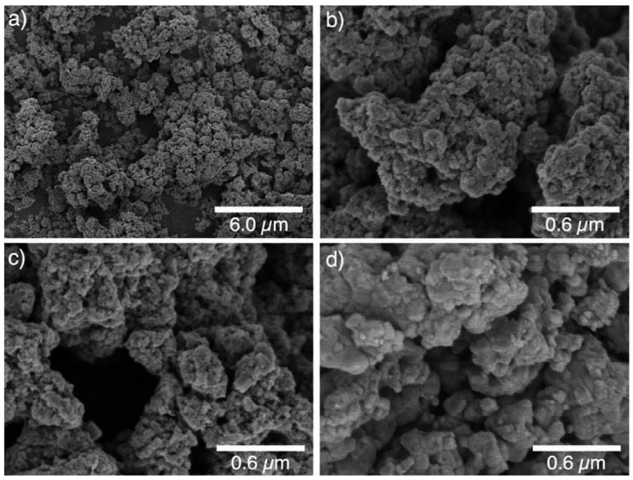

Fig. 2 SEM images of (a), (b) LTO/C-3, (c) LTO/C-9 and (d) C-LTO-0.

The textural properties of LTO/C nanocomposites were measured by N_2 adsorption–desorption. As shown in Table 2, the specific surface area of the materials increases with the carbon content, while the pore volume remains practically constant, suggesting that the carbon phase is microporous and participates significantly to the textural properties of the nanocomposite. In the case of LTO/C-0, the surface area is negligible. This loss of specific surface area can be ascribed to the removal of the porous carbon phase and also to the sintering of the naked LTO particles, as suggested by SEM images (see below).

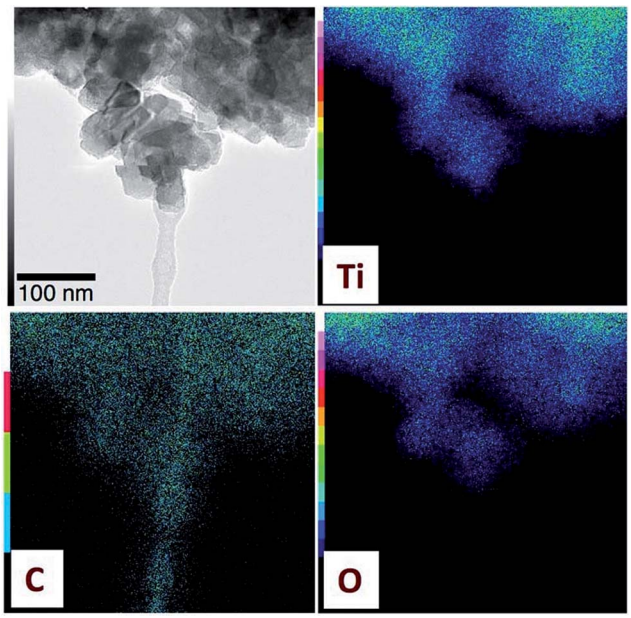

Fig. 3 TEM images of LTO/C-3 with EDX mapping, confirming a homogeneous dispersion of all elements (C, Ti and O).

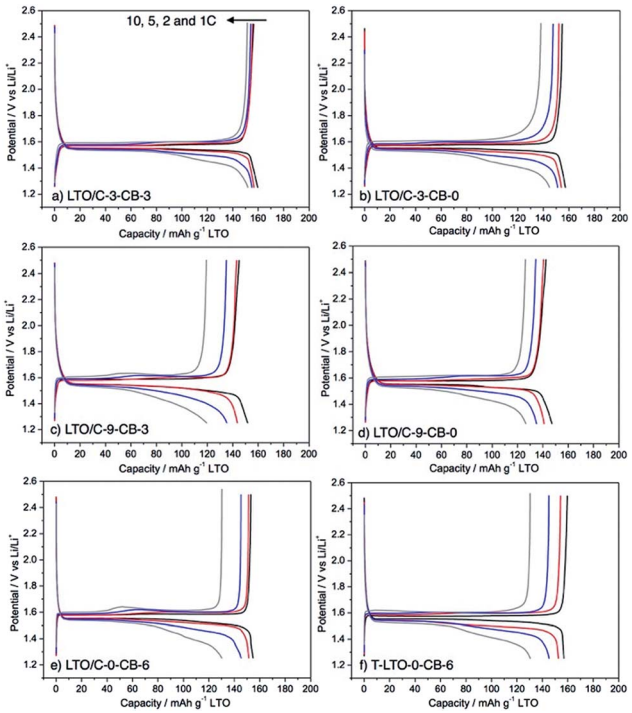

Fig. 4 Representative galvanostatic charge–discharge voltage profiles (1.25 to 2.5 V) of LTO electrodes at different current densities (2nd cycle for each current density) of (a) LTO/C-3-CB-3, (b) LTO/C-3-CB-0, (c) LTO/C-9-CB-3, (d) LTO/C-9-CB-0, (e) LTO/C-0-CB-6 and (f) T-LTO-CB-6.

The morphology of LTO/C nanocomposites was investigated using SEM (Fig. 2) and TEM analysis (Fig. 3). All nanocomposites consisted of aggregated nanoparticles (*ca.* 30 nm in size). After removal of the carbon by calcination at 500 °C (LTO/C-0), the surface of LTO particles became smoother, suggesting a sintering of the particles. Considering the densities of LTO (3.43 g cm^{-3}) and amorphous carbon (1.8–2.1 g cm^{-3}), the volume fraction of carbon in samples LTO/C-3 and LTO/C-9 are

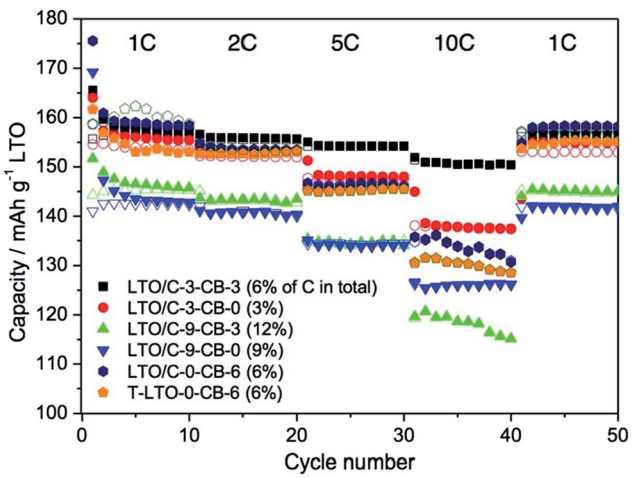

Fig. 5 Rate-capability and cycling performance of LTO/C electrode materials, compared to commercial T-LTO material. Filled and open symbols refer to reduction (discharge) and oxidation (charge), respectively.

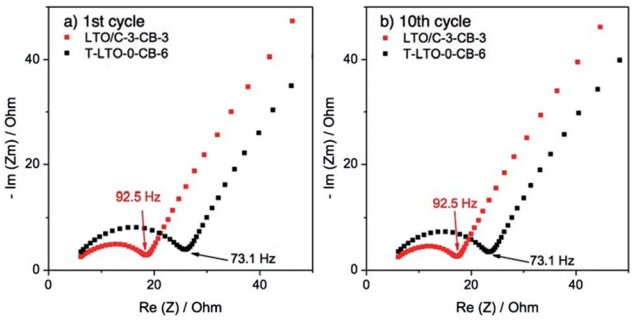

Fig. 6 The Nyquist plots for LTO/C-3-CB-3 and T-LTO-0-CB6 at (a) 1st cycle and (b) 10th cycle.

≈5 and ≈15%, respectively. However, no independent carbon phase was detected by SEM, even for the LTO/C-9 sample, suggesting that the carbon forms a thin coating over the LTO particles. This was confirmed using TEM-EDX mapping (Fig. 3). The distribution of Ti, O and C coincide, indicating a homogeneous dispersion of carbon at the surface of LTO particles.

Electrochemical performance of LTO/carbon nanocomposites

The electrochemical performance of LTO/C-3 and LTO/C-9 nanocomposites and the influence of the addition of carbon black (Super P) were investigated by preparing electrodes with different amount of carbon black (3 wt% and 0 wt%) which were tested in coin-type half-cells *vs.* Li metal within a potential window of 1.25 to 2.5 V. The electrodes are labelled LTO/C-*x*-CB-*y*, as explained in the experimental part. For comparison, electrodes based on LTO/C-0 and T-LTO formulated with 6 wt% carbon black were also investigated (electrodes LTO/C-0-CB-6 and T-LTO-CB-6).

The galvanostatic charge–discharge voltage profiles of the electrodes are displayed in Fig. 4, their rate-capability and cycling performance in Fig. 5. At the initial current density (1C) the galvanostatic curve of all electrodes displayed a specific plateau around 1.55 V *vs.* Li^+/Li, which is typical of LTO and is classically attributed to the coexistence of 2 phases, $Li_4Ti_5O_{12}$ and $Li_7Ti_5O_{12}$.[31] As shown in Fig. 5, after 10 cycles at 1C the specific capacities of LTO in electrodes derived from LTO/C-3 (157 mA h g^{-1} for LTO/C-3-CB-0, 155 mA h g^{-1} for LTO/C-3-CB-3) were close to the specific capacity of the electrode derived from the commercial LTO (153 mA h g^{-1} for T-LTO-CB-6). At high current densities, the LTO/C-3-CB-3 electrode

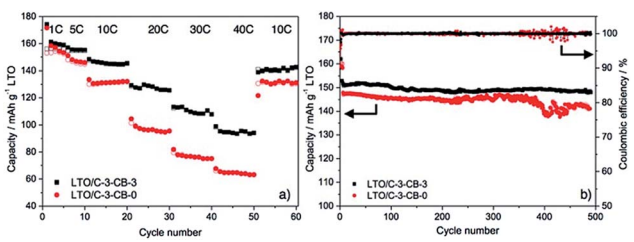

Fig. 7 (a) Rate capability and (b) long term cyclability performance of LTO/C-3 based electrodes.

Table 3 Performances of selected $Li_4Ti_5O_{12}$ materials as anode in Li ion batteries

Type of material	Synthetic method	Carbon content in composites (wt%)	Carbon content in electrode formulation (wt%)	Specific capacity (mA h g^{-1})	High rate capacity (mA h g^{-1})	Cycliability (capacity retention %)	Ref.
$Li_4Ti_5O_{12}$/carbon nanocomposite	Solid state reaction of TiO_2, LiOAc with aqueous gel of alginic acid as carbon source	3	3	155 mA h g^{-1} at 1C	152 mA h g^{-1} at 10C 95 mA h g^{-1} at 40C	97.5% at 5C for 500 cycles	This work
$Li_4Ti_5O_{12}$/hollow graphitized nano-carbon composites	Hydrothermal synthesis using TiO_2, LiOH and hollow graphitized nano-carbon	10	10	162 mA h g^{-1} at 0.32C	105 mA h g^{-1} at 32C	91.2% at 16C for 500 cycles	16
$Li_4Ti_5O_{12}$/mesoporous carbon composite	Impregnation of LTO precursors, $Ti(OC_4H_9)_4$ and LiOAc into mesoporous carbon	16	2	162 mA h g^{-1} at 0.2C	93 mA h g^{-1} at 40C	94.4% at 20C for 1000 cycles	14[a]
Carbon coated $Li_4Ti_5O_{12}$ nanoparticles	Solid state reaction of TiO_2, Li_2CO_3 with sucrose as carbon source	Not mentioned	8	171 mA h g^{-1} at 0.5C	150 mA h g^{-1} at 12.5C 82 mA h g^{-1} at 75C	98% at 75C for 300 cycles	22
Carbon coated $Li_4Ti_5O_{12}$ nanoparticles	Solid state reaction of TiO_2, Li_2CO_3 with polyacrylate acid as carbon source	3.5	10	168 mA h g^{-1} at 0.2C	132 mA h g^{-1} at 10C	97.2% at 0.2C for 50 cycles	23[a]
Carbon coated $Li_4Ti_5O_{12}$ nanoparticles	Sol–gel synthesis using $Ti(OC_4H_9)_4$, LiOAc with glycine as carbon source	1.0	15	168 mA h g^{-1} at 1C	145 mA h g^{-1} at 10C 99 mA h g^{-1} at 50C	83% at 10C for 1500 cycles	32[a]
Carbon coated $Li_4Ti_5O_{12}$ nanoparticles	Sol–gel synthesis using $Ti(OC_4H_9)_4$, LiOAc with citric acid as carbon source	1.3	10	165 mA h g^{-1} at 2.5C	147 mA h g^{-1} at 50C	98% at 50C for 50 cycles	34
Carbon coated $Li_4Ti_5O_{12}$ microsphere	Solid state reaction of TiO_2, Li_2CO_3 with pitch	5.2	10	165 mA h g^{-1} at 3.3C	120 mA h g^{-1} at 33C	>99% at 3.3C for 100 cycles	35
Nano-sized $Li_4Ti_5O_{12}$	Solid state reaction of TiO_2, Li_2CO_3	0	10	164 mA h g^{-1} at 1C	129 mA h g^{-1} at 10C	95% at 1C for 100 cycles	36[a]
Porous $Li_4Ti_5O_{12}$	Sol–gel synthesis using LiCl and $TiCl_4$ with oxalic acid as morphology control agent	0	13	167 mA h g^{-1} at 1.6C	70 mA h g^{-1} at 33C	98% at 3.3C for 200 cycles	26

[a] In these papers, the current density corresponding to 1C was not clearly defined. For the others, the current density was recalculated using 1C = 58.3 mA g^{-1}.

performed significantly better than the other electrodes, retaining after 10 cycles at 10C a specific capacity of 152 mA h g^{-1}, *i.e.* more than 95% of its capacity at 1C. The capacity retention for LTO/C-3-CB-0 was lower, ≈88%. In comparison, the electrode based on commercial LTO (T-LTO-CB-6) showed only 84% of capacity retention, even with 6 wt% of carbon black. The LTO derived from LTO/C-3 by calcination (LTO/C-0-CB-6 electrode, ≈83% of capacity retention) behaved in a similar way as the commercial LTO.

The excellent performances of electrodes based on the LTO/C-3 nanocomposite can be explained as follows: first, as already shown in TEM images, the carbon is homogenously dispersed over the LTO aggregated particles, ensuring better electronical connection between particles compared to the carbon black additive. Moreover, the porosity of this carbon coating should also provide easy access of the electrolyte to the surface. Indeed, a non porous, continuous carbon coating could hinder the access of the electrolyte to the active material surface.[32,33] Finally, Li^+ insertion and de-insertion kinetics is expected to be faster for LTO/C nanocomposite than for T-LTO as the LTO particle size in the nanocomposites (≈30 nm) is significantly lower than in T-LTO (≈200 nm) (Fig. S2†).

A higher carbon content in the nanocomposite does not lead to better performances. Thus, the specific capacity of LTO for LTO/C-9-CB-3 or LTO/C-9-CB-0 electrodes was lower than that of electrodes based on LTO/C-3 and T-LTO (Fig. 4c and 5). In addition, as shown in Fig. S3,† the performance of a nanocomposite with 19 wt% of C were even worse (only 125 mA h g^{-1} of specific capacity of LTO after 10 cycles at 1C). This behaviour suggests that a high carbon content could impede Li^+ ion transfer onto the LTO surface. Thus, the presence of intrinsic carbon in the nanocomposite is essential, but a high amount of carbon should be avoided for better performance. In addition, for practical application, a higher carbon content will increase the weight and thus decrease the volumetric capacity of the battery.

Electrochemical impedance spectroscopy (EIS) analysis was carried out on LTO/C-3-CB-3 and T-LTO-0-CB-6, which have the same amount of carbon in the final electrode formulation. Nyquist plots (Fig. 6) for both electrodes show a single semicircle in the middle to high frequency range, which is attributed to the charge transfer resistance (R_{ct}) between electrolyte and LTO. The charge transfer resistance (R_{ct}) for LTO/C-3-CB-3 at 1st and 10th cycle for LTO/C-3-CB-3 is obviously smaller than R_{ct} for T-LTO-0-CB-6, which suggests that the carbon in composite could decrease the resistance more effectively than carbon black.

Finally, the performance at high rate (up to 40C) and the long-term cyclability were investigated for the LTO/C-3 nanocomposite, which showed the best electrochemical performances among LTO/C materials. As shown in Fig. 7a, at 40C the LTO/C-3-CB-3 electrode retained a specific capacity for LTO of 95 mA h g^{-1}, around 60% of the specific capacity at 1C. Interestingly, the LTO/C-3 electrode without carbon additive (LTO/C-3-CB-0) also showed good rate capability performance, 63 mA h g^{-1} at 40C. For long term cyclability (Fig. 7b), LTO/C-3-CB3 showed a discharge capacity of 151 mA h g^{-1} after 500 cycles at 5C, with only 2.5% capacity loss compared to the first cycle. The coulombic efficiency remained constant at 98.7% after 500 cycles, demonstrating an excellent reversibility of Li^+ insertion and de-insertion. The C-LTO-3-CB-0 electrode, despite a moderate drop of the capacity after *ca.* 400 cycles, still showed good long term cyclability performance at 5C.

Comparison with the literature (Table 3) shows that the performance of our LTO/C nanocomposites is better than that of LTO/C composites prepared by solid-state reaction, and comparable with that of LTO/C composites synthetized by more sophisticated methods such as sol–gel synthesis. In addition, the total carbon content in our case (3 to 6 wt%) is significantly lower than in the other examples (10 to 20 wt%). Thus, considering the simplicity and low cost of the synthesis, the LTO/C nanocomposites described in this study could be a promising candidate as anode material for practical application in lithium-ion batteries.

Conclusions

In conclusion, we have developed a simple one-pot synthesis of LTO/C nanocomposites using an alginic acid aquagel as carbon source and chelating agent, and LiOAc and TiO_2 particles as LTO precursors. The carbon appears homogenously dispersed over the aggregated LTO nanoparticles, forming a porous coating. The nanocomposite with a moderate amount of carbon (3 wt%) showed promising performances as a negative electrode material for lithium ion batteries, leading to high rate capability and long term cyclability even with a low amount of carbon black as a conductive additive. Therefore, these LTO/carbon nanocomposites could find applications in high-power lithium-ion batteries, for instance, for electrical vehicles or for stationary energy storage systems with longer lifespan.

Conflicts of interest

There are no conflicts to declare.

Acknowledgements

Financial support was received by the European Commission in the framework of POROUS4APP project (H2020 GA no. 666157). The authors would like to thank Didier Cot (IEM, France) for SEM analysis. Lea Daenens (ICGM, France) is gratefully acknowledged for technical help in the collection of the Raman spectra.

Notes and references

1 T. Yuan, Z. Tan, C. Ma, J. Yang, Z.-F. Ma and S. Zheng, *Adv. Energy Mater.*, 2017, **7**, 1601625.
2 T. Ohzuku, *J. Electrochem. Soc.*, 1995, **142**, 1431–1439.
3 T.-F. Yi, S.-Y. Yang and Y. Xie, *J. Mater. Chem. A*, 2015, **3**, 5750–5777.
4 X. Sun, P. V. Radovanovic and B. Cui, *New J. Chem.*, 2014, **39**, 38–63.

5 T.-F. Yi, L.-J. Jiang, J. Shu, C.-B. Yue, R.-S. Zhu and H.-B. Qiao, *J. Phys. Chem. Solids*, 2010, **71**, 1236–1242.
6 T.-F. Yi, Y. Xie, Y.-R. Zhu, R.-S. Zhu and H. Shen, *J. Power Sources*, 2013, **222**, 448–454.
7 Y. Ma, B. Ding, G. Ji and J. Y. Lee, *ACS Nano*, 2013, **7**, 10870–10878.
8 X. Han, Z. Zhao, Y. Xu, D. Liu, H. Zhang and C. Zhao, *RSC Adv.*, 2014, **4**, 41968–41975.
9 J.-G. Kim, M.-S. Park, S. M. Hwang, Y.-U. Heo, T. Liao, Z. Sun, J. H. Park, K. J. Kim, G. Jeong, Y.-J. Kim, J. H. Kim and S.-X. Dou, *ChemSusChem*, 2014, **7**, 1451–1457.
10 G.-N. Zhu, H.-J. Liu, J.-H. Zhuang, C.-X. Wang, Y.-G. Wang and Y.-Y. Xia, *Energy Environ. Sci.*, 2011, **4**, 4016–4017.
11 T.-F. Yi, Z.-K. Fang, Y. Xie, Y.-R. Zhu and S.-Y. Yang, *ACS Appl. Mater. Interfaces*, 2014, **6**, 20205–20213.
12 E. Kang, Y. S. Jung, G.-H. Kim, J. Chun, U. Wiesner, A. C. Dillon, J. K. Kim and J. Lee, *Adv. Funct. Mater.*, 2011, **21**, 4349–4357.
13 F. Zhang, B. Xu, G. Cao, M. Chu, N. Qiao, G. Wei and Y. Yang, *RSC Adv.*, 2014, **4**, 53981–53986.
14 L. Shen, X. Zhang, E. Uchaker, C. Yuan and G. Cao, *Adv. Energy Mater.*, 2012, **2**, 691–698.
15 S. D. Kim, K. Rana and J.-H. Ahn, *J. Mater. Chem. A*, 2016, **4**, 19197–19206.
16 L. Fan, X. Tan, T. Yu and Z. Shi, *RSC Adv.*, 2016, **6**, 26406–26411.
17 C.-M. Chang, Y.-C. Chen, W.-L. Ma, P.-H. Wang, C.-F. Lee, H.-S. Chen and Y. W. Chen-Yang, *RSC Adv.*, 2015, **5**, 74381–74390.
18 A. Nugroho, W. Chang, S. Jin Kim, K. Yoon Chung and J. Kim, *RSC Adv.*, 2012, **2**, 10805.
19 H. Ge, T. Hao, H. Osgood, B. Zhang, L. Chen, L. Cui, X.-M. Song, O. Ogoke and G. Wu, *ACS Appl. Mater. Interfaces*, 2016, **8**, 9162–9169.
20 E. Zhao, C. Qin, H.-R. Jung, G. Berdichevsky, A. Nese, S. Marder and G. Yushin, *ACS Nano*, 2016, **10**, 3977–3984.
21 Y. Shen, M. Søndergaard, M. Christensen, S. Birgisson and B. B. Iversen, *Chem. Mater.*, 2014, **26**, 3679–3686.
22 X. Guo, H. F. Xiang, T. P. Zhou, X. K. Ju and Y. C. Wu, *Electrochim. Acta*, 2014, **130**, 470–476.
23 X. Hu, Z. Lin, K. Yang, Y. Huai and Z. Deng, *Electrochim. Acta*, 2011, **56**, 5046–5053.
24 C.-H. Hong, A. Noviyanto, J. H. Ryu, J. Kim and D.-H. Yoon, *Ceram. Int.*, 2012, **38**, 301–310.
25 L. Yang and L. Gao, *J. Alloys Compd.*, 2009, **485**, 93–97.
26 C.-Y. Lin and J.-G. Duh, *J. Alloys Compd.*, 2011, **509**, 3682–3685.
27 R. J. White, C. Antonio, V. L. Budarin, E. Bergström, J. Thomas-Oates and J. H. Clark, *Adv. Funct. Mater.*, 2010, **20**, 1834–1841.
28 Y. Sha, X. Xu, L. Li, R. Cai and Z. Shao, *J. Power Sources*, 2016, **314**, 18–27.
29 J. Yan, G. Wu, N. Guan, L. Li, Z. Li and X. Cao, *Phys. Chem. Chem. Phys.*, 2013, **15**, 10978–10988.
30 B. Fang, M.-S. Kim, J. H. Kim, S. Lim and J.-S. Yu, *J. Mater. Chem.*, 2010, **20**, 10253–10259.
31 S. Scharner, W. Weppner and P. Schmid-Beurmann, *J. Electrochem. Soc.*, 1999, **146**, 857–861.
32 X. Guan, X. Chen, G. Li, Y. Zang, H. Lin, D. Luo and L. Li, *RSC Adv.*, 2013, **3**, 3088–3094.
33 R. Dominko, M. Bele, M. Gaberscek, M. Remskar, D. Hanzel, S. Pejovnik and J. Jamnik, *J. Electrochem. Soc.*, 2005, **152**, A607–A610.
34 Y.-C. Kuo and J.-Y. Lin, *Electrochim. Acta*, 2014, **142**, 43–50.
35 H.-G. Jung, S.-T. Myung, C. S. Yoon, S.-B. Son, K. H. Oh, K. Amine, B. Scrosati and Y.-K. Sun, *Energy Environ. Sci.*, 2011, **4**, 1345–1351.
36 X. Li, H. Hu, S. Huang, G. Yu, L. Gao, H. Liu and Y. Yu, *Electrochim. Acta*, 2013, **112**, 356–363.